Appl. Phys. B (2014) 116:763–769
DOI 10.1007/s00340-013-5759-9

Applied Physics B
Lasers and Optics

Phase-dependent spectral control of pulsed modulation instability via dichromatic seed fields

Maximilian Brinkmann · Michael Kues · Carsten Fallnich

Received: 30 September 2013 / Accepted: 30 December 2013 / Published online: 16 January 2014

Abstract We investigated experimentally and numerically the spectral control of modulation instability (MI) dynamics via the initial phase relation of two weak seed fields. Specifically, we show how second-order MI dynamics exhibit phase-dependent anti-correlated growth rates of adjacent spectral sidebands. This effect enables a novel method to control MI-based frequency conversion: in contrast to first-order MI dynamics, which exhibit a uniform phase dependence of the growth rates, second-order MI dynamics allow to redistribute the spectral energy, leading to an asymmetric spectrum. Therefore, the presented findings should be very attractive to different applications, such as phase-sensitive amplification or supercontinuum generation initiated by MI.

1 Introduction

Modulation instability (MI) [1], describing the exponential amplification of a weak modulation on a strong pump field background in a nonlinear dispersive medium, is spectrally characterized by a drastic energy transfer from the pump's carrier frequency ν_0 into spectral sidebands around ν_0. Experimentally, this process can be induced by superimposing the pump field with a weak seed field, frequency-shifted relative to ν_0, to imprint a defined initial modulation on the pump's amplitude. In this way, initiated by a weak coherent signal, MI is exploited, e.g., for ultrashort pulse train generation [2] or in seeded supercontinuum generation [3].

M. Brinkmann (✉) · M. Kues · C. Fallnich
Institute of Applied Physics, Westfälische Wilhelms-Universität Münster, Corrensstraße 2, 48149 Münster, Germany
e-mail: brinkmannmax@wwu.de

When seeding with a single-frequency mode, the MI evolution can be controlled via the amplitude of the seed field and via the frequency shift of the seed field, defining the spectral positions of the sidebands. As pointed out in reference [4], the MI evolution can furthermore be spectrally controlled via the pump–seed phase relation, when excited by two seed frequencies symmetrically spaced around ν_0. Specifically, a first-order MI excited by two symmetrically placed seed frequencies exhibits symmetric sideband growth depending on the pump–seed phase relation, providing a possibility to change the amplitudes of all sidebands in equal measure. In contrast to the conditions stated above, a second-order MI is excited, if a modulation composed of two frequencies is imprinted on the pump's amplitude. Most formally this can be accomplished via two pairs of seed frequencies, both partners of each pair symmetrically placed around ν_0 and within the MI gain bandwidth [5]. Nevertheless, only two non-conjugated seed frequencies within the MI gain bandwidth are sufficient to excite second-order MI dynamics. Thus, for experimental simplicity in this paper, we consider only two seed frequencies that are spectrally located together only on the low-frequency side of the carrier frequency to excite second-order MI dynamics. Furthermore, our numerical model indicated that this seed configuration enables the most sensible and yet effective phase dependency of the resulting spectral evolution.

We show numerically and experimentally that second-order MI dynamics excited with this approach exhibit an anti-symmetric phase dependence of the growth rates, meaning that the growth rates of two sidebands, which form a sideband pair, vary anti-correlated with the initial phase. This presented effect enables a novel method to control MI-based frequency conversion and should therefore be attractive to different applications.

The nonlinear element required for the excitation of such MI dynamics was chosen to be a microstructured fiber (NL-PM-750, NKT-Photonics). Furthermore, in order to circumvent high continuous-wave powers, we used pulsed pump and seed fields to excite MI dynamics, which is a common method, especially in investigations on MI-based supercontinuum generation [6]. Note that MI dynamics ultimately lead to a fission of the pump pulse after a certain propagation distance into individual soliton-like subpulses due to disruption by higher-order dispersion and Raman scattering [7]. After the fission of the pulse, the optical field dynamics are not governed by MI anymore; thus, we limited our investigations to the dynamics before the onset of pulse fission.

This paper is structured as follows: first, the applied numerical model is outlined in Sect. 2, the used experimental setup is presented in Sect. 3, subsequently, the uniform phase dependence of the growth rates of first-order MI is experimentally verified in Sect. 4, and the investigation on second-order-like MI is presented in Sect. 5.

2 Numerical model

In order to model and numerically investigate MI dynamics in a microstructured fiber, we used the generalized scalar nonlinear Schrödinger equation (GNLSE), which has been proven many times to accurately describe nonlinear unidirectional pulse propagation in MSF [7]. Explicitly including higher-order linear and nonlinear terms, we used the GNLSE in the following form [7]:

$$\frac{\partial A}{\partial z} = -\frac{\alpha}{2}A + \sum_{k\geq 2}^{10} \frac{i^{k+1}}{k!}\beta_k \frac{\partial^k A}{\partial t^k} + i\gamma\left(1 + i\frac{1}{2\pi\nu_0}\frac{\partial}{\partial t}\right) \cdot \left(A(z,t)\int_{-\infty}^{\infty} R(t')|A(z,t-t')|^2 \mathrm{d}t'\right). \quad (1)$$

Considering the slowly varying envelope approximation, here, $A(z, t)$ describes the pulse envelope and t is the time in a frame of reference moving with the group velocity $\frac{1}{\beta_1}$. The values β_k are the dispersion coefficients at the center frequency ν_0, and α and γ are the absorption and nonlinear coefficients of the fiber. The response function $R(t) = (1 - f_R)\delta(t) + f_R \ h_R(t)$ with $f_R = 0.18$ includes both instantaneous electronic and delayed Raman contributions, whereby we used the analytic form of the Raman response function [8]: $h_R(t) = [(\tau_1^2 + \tau_2^2)/(\tau_1\tau_2^2)]\exp(-t/\tau_2)\sin(t/\tau_1)$ with $\tau_1 = 12.2$ and $\tau_2 = 32$ fs.

We solved the GNLSE numerically stepwise along the fiber by means of a split-step Fourier method [9], considering a step size of 10 μm, an array size of 2^{16} points and a temporal resolution of 0.5 fs. The modeled fiber input fields constituted superpositions of sech^2-shaped pulses, representing the pump and seed pulses. In order to investigate the field evolution depending on the relative phase between the pump and the seed pulses, the phase of the pump pulse was varied by multiplying time-independent phase terms to the initial pump pulse, while keeping the phase of the seed fields constant. Thus, the following investigations were concentrated only on the effect of the relative phase between the pump and both seed pulses, whereby the relative phase between the two seed pulses was not varied. Indeed, by means of our numerical model, we were able to verify that the field evolution is determined by the phases of all three interacting pulses relative to each other. However, varying the phase of the pump pulse accomplished the simplest and most effective spectral control of the MI dynamics. Therefore, we restricted our investigations to control the individual sidebands in a correlated or anti-correlated way on the relative phase of the pump pulse.

3 Experimental setup

A schematic of the experimental setup is shown in Fig. 1: the microstructured fiber (NL-PM-750, NKT-Photonics) used to investigate MI dynamics had a length of 25 cm, the nonlinear coefficient was $\gamma = 0.095$ /(Wm), and the second-order dispersion was $\beta_2 = -0.5812$ ps^2/cm at 384.5 THz, i.e., at a wavelength of 782 nm. To allow for mutually coherent pump and seed fields, a mode-locked titanium–sapphire laser was used, emitting bandwidth-limited pulses with a duration of 80 fs (FWHM) at a center frequency of 384.5 THz. The pump pulses were generated by stretching the laser output pulses to a temporal duration of 1.8 ps, necessary to suppress self-phase modulation within the fiber so that a field evolution dominated by MI was ensured. The pulse stretching was accomplished by employing normal dispersion via a folded Martinez stretcher [10], consisting of a cylindrical lens ($f = 100$ mm) and a transmission grating (1,200 lines/mm). In this way, the fiber was pumped with a chirped pulse in the anomalous dispersion regime. However, we spend no further attention to the pulse chirp as we were able to verify by numerical investigations that a pulse chirp does not alter the phase dependence of the MI evolution.

To generate the seed fields, replicas of the laser output pulses produced with a beam splitter (BS 1) were focused into an additional segment ($\mathrm{MSF_{SC}}$, length of 3 cm) of the mentioned microstructured fiber to allow for coherent supercontinuum generation by exploiting soliton dynamics. The seed fields were then synthesized by cutting the desired frequencies out of the supercontinuum spectrum

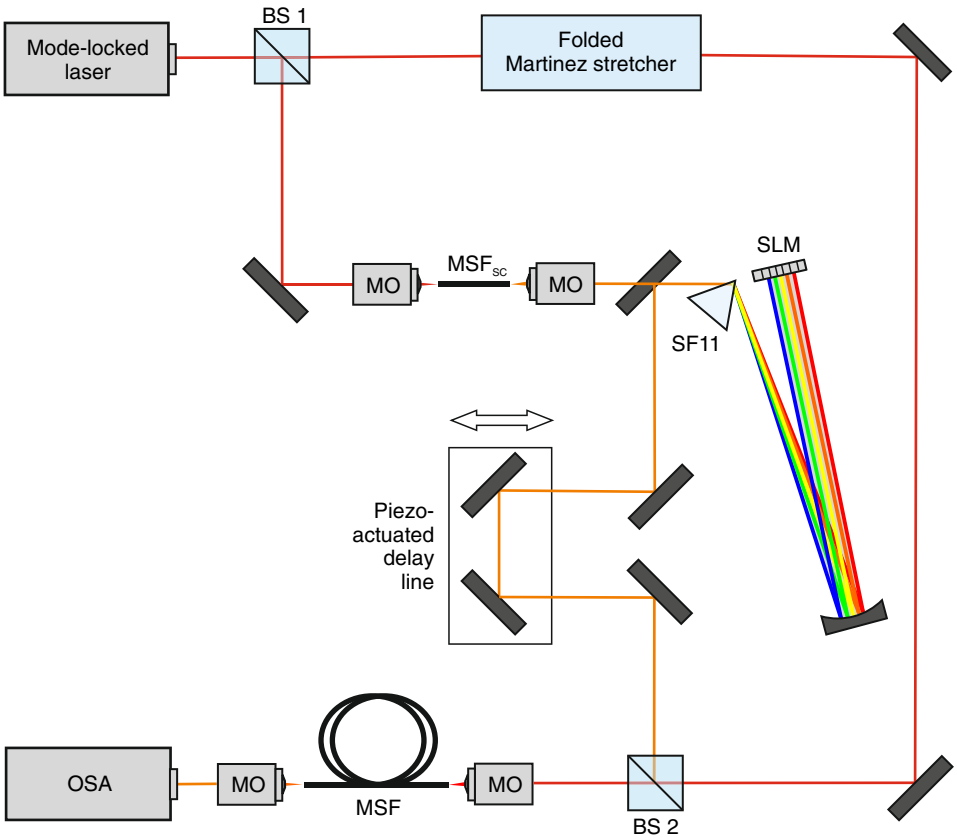

Fig. 1 Schematic diagram of experimental setup. *BS* beam splitter, *MO* microscope objective, *MSF* microstructured fiber used to investigate MI dynamics, MSF_{SC} microstructured fiber used to generate supercontinuum pulses, *SLM* spatial light modulator, *OSA* optical spectrum analyzer

using a spectral pulse shaper based on a SF11 prism and a liquid crystal spatial light modulator (SLM).

Before the pump field and the seed fields were combined and simultaneously injected via a 40× microscope objective into the microstructured fiber to excite MI dynamics, the pump field passed a piezo-actuated retroreflector enabling phase changes between the pump and seed fields. The spectra of the fiber output pulses were measured with an optical spectrum analyzer.

4 First-order modulation instability

Figure 2 shows a measured unseeded fiber output spectrum (red dashed line) for an estimated pump peak power of $P_0 = 300$ W and the associated MI gain [7] (black dashed line). In contrast to this unseeded case, the measured spectrum illustrated by the blue solid line was generated by the pump field superimposed with a single seed field, whose center frequency of 374.0 THz was located within the gain bandwidth. The average seed power was about 1,000 times smaller than the average pump power of about 45 mW. The single seed field stimulated a cascaded generation of sidebands around the pump frequency. Specifically, the spectrum of the seeded case shows three pairs of sidebands, which are spectrally separated by the induced

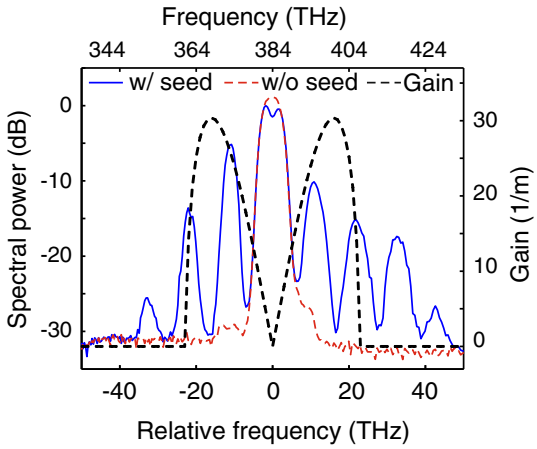

Fig. 2 Measured spectra without (*red dashed line*) and with seed (*blue solid line*) at $\nu_{-1} = -10.5$ THz, as well as MI gain curve for the used fiber and pump pulse peak power (*black dashed line*)

modulation frequency $\Omega = 10.5$ THz, clearly exposing a successful excitation of pulsed MI. However, in contrast to the commonly known symmetric MI spectra [11] generated by continuous pump and seed fields, the spectrum in Fig. 2 shows an additional sideband standing alone on the high-frequency side of the pump frequency mode at about 42 THz without a partner on the low-frequency side. We were able to attribute this symmetry breaking by means of

numerical simulations to effects of higher-order dispersion. A similar symmetry breaking of the MI spectrum has been observed before and has been accounted for by a decreased phase mismatch between the pump frequency and higher-order sidebands on the high-frequency side of the pump compared with the phase mismatch between the pump frequency and sidebands on the low-frequency side of the pump. The reason for this asymmetry was found in the effect of third-order dispersion [12, 13]. Nevertheless, the pump frequency mode in the spectrum of the seeded case is furthermore depleted compared with the spectrum of the unseeded case, which is another characteristic of MI owing to the energy transfer into the sidebands. In the following, these sidebands shall be denoted relative to ν_0 by their frequency shift: $\nu_n = n \cdot \Omega$ with $n = \pm1, \pm2, \pm3, \ldots$.

The experimentally induced MI dynamics could also be modeled accurately with our numerical model: considering the above-presented experimental parameters, simulations yielded the dash-drawn spectrum in Fig. 3. Besides the measured and simulated spectra, Fig. 3 furthermore illustrates the notation of the sidebands. It can be seen that the amplitude levels of the measured and simulated spectra do not coincide accurately, which can be accounted for by inaccuracies in the experimental parameters: especially the seed field's temporal duration and peak power could only be approximated because of the low peak power. However, as the measured spectral position of the sidebands is well reproduced by the simulations, and as we are only interested in relative amplitude changes, the simulations constitute an adequate tool for estimation and comparison.

Based on this agreement, in a first step, numerical investigations focusing on a spectral phase dependence were performed, considering a pump peak power of $P_0 = 300$ W (average power of $\bar{P}_0 = 45$ mW) and a single seed at $\nu_{-1} = -10.5$ THz with an average power of $\bar{P}_{\text{Seed}} = \frac{1}{1{,}000}\bar{P}_0$. Note that only the average power of the seed pulse is stated as the peak power of the pulse could only be estimated. However, considering a spectral width of the seed pulse of 8 nm (corresponding to a bandwidth-limited duration of 80 fs), an upper limit of 7 W for the seed peak power can be specified. For this case, Fig. 4a shows the intensities of the first two sideband pairs as a function of the phase of the pump. All sideband intensities remain constant; thus, a phase dependence is not observable. As derived analytically in Ref. [5], in this case of initial conditions, consisting of only a pump frequency ν_0 and a single seed frequency ν_-1, the frequency mode ν_1, conjugated to ν_{-1}, is generated during the initial propagation through the fiber by the process of MI itself. Thereby, the phase of the generated frequency mode ν_1 is set automatically such that the relative phase difference between ν_0 and $\nu_{\pm1}$ is $\frac{\pi}{2}$, which yields maximum growth rates. Thus, in this case, the phase of the generated frequency mode ν_1 is determined by the two initial frequencies ν_0 and ν_{-1}, which leads to a phase-independent MI evolution.

In contrast, Fig. 4b contains the same diagram but for two seed fields at frequencies of $\nu_{-1} = -10.5$ THz and $\nu_1 = 10.5$ THz; both are lying under the MI gain curve and are fulfilling the frequency relation $\nu_{-1} = -\nu_1$. Here, the sideband intensities vary synchronously, attesting phase-dependent but positively correlated growth rates of the sidebands. This numerically revealed phase dependency in

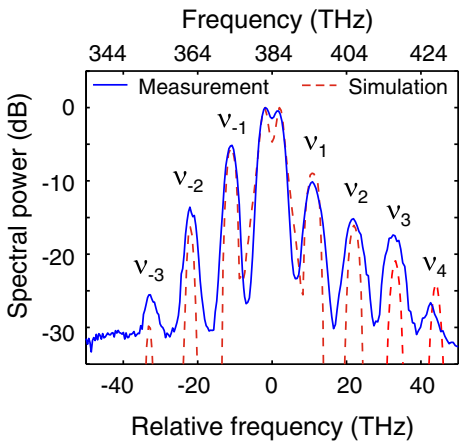

Fig. 3 Measured (*blue solid line*) and simulated (*red dashed line*) spectra with seed at $\nu_{-1} = -10.5$ THz

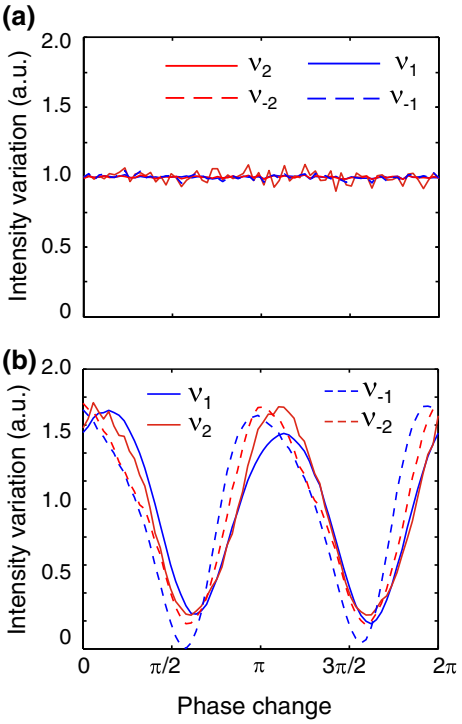

Fig. 4 Simulated intensity variation of sidebands $\nu_{\pm1}$, $\nu_{\pm2}$, seeded with **a** one seed field at $\nu_{-1} = -10.5$ THz and **b** two seed fields at $\nu_{-1} = -10.5$ THz and $\nu_1 = 10.5$ THz

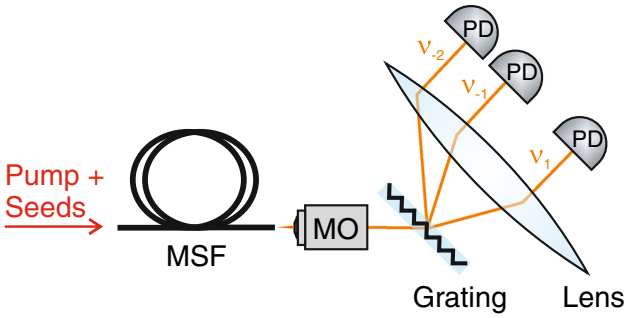

Fig. 5 Setup to measure phase-dependent variations of the intensities of the first three sideband modes ($\nu_{\pm 1}$, ν_{-2}) of the fiber output spectrum. *MO* microscope objective, *MSF* microstructured fiber, *PD* photodetector

case of two symmetrically placed seed frequency is in accordance with analytical investigations of reference [5]. We were able to attribute the slight phase shifts between the four displayed curves by numerical simulations (not shown here) to higher-order dispersion and Raman effects.

To allow for an appropriate experimental measurement of the variation of the sidebands' intensities as a function of the phase of the pump pulses, the phase of the pump pulses was varied by modulating the piezo with a sinusoidal function, fast enough to neglect fluctuations of the interferometric setup caused by external mechanical or thermal perturbations over the measurement time. In this way, phase-dependent effects could be investigated without an active stabilization of the setup. However, in order to measure the resulting rapid phase-dependent spectral changes, the slow optical spectrum analyzer had to be replaced with the setup illustrated in Fig. 5: the spectral components of the fiber output were spatially dispersed employing a grating (1,200 lines/mm), and the sideband modes $\nu_{\pm 1}$ and ν_{-2} were individually focused onto separate fast silicon photodetectors (150-MHz bandwidth). All detectors were connected to an oscilloscope (1-GHz bandwidth). Due to the limited number of channels of this oscilloscope, only the intensities of the mentioned first three sidebands could be measured. Synchronously to the sidebands' intensities, the piezo voltage was measured, allowing, in combination with a calibration of the delay induced by the piezo, for a reconstruction of the phase variation.

For seeding the MI with only a single-frequency mode at $\nu_{-1} = -10.5$ THz and the same parameters as above, Fig. 6a shows the detected signals of the sidebands normalized to their own mean value as a function of the phase variation. In accordance with the simulations, the intensities of the sidebands do not change. However, with the injection of a second seed at a frequency of $\nu_1 = 10.5$ THz into the fiber, a change of the sidebands' intensities becomes clearly visible as illustrated in

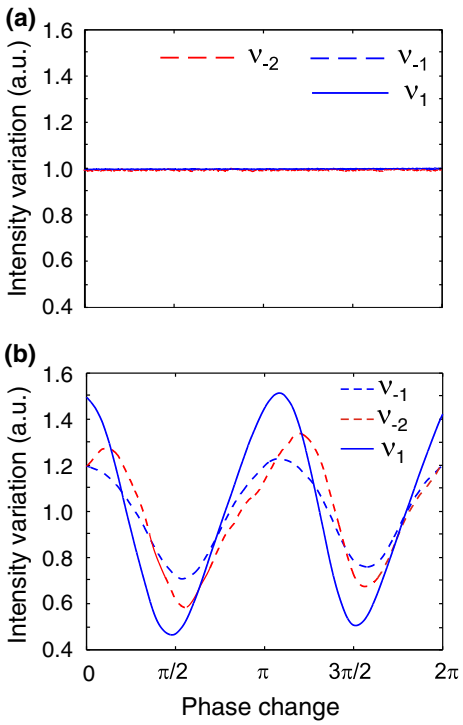

Fig. 6 Measured intensity variation of sidebands $\nu_{\pm 1}$, ν_{-2}, seeded with **a** one seed field at $\nu_{-1} = -10.5$ THz and **b** two seed fields at $\nu_{-1} = -10.5$ THz and $\nu_1 = 10.5$ THz , as a function of the phase shift of the seed fields relative to the pump

Fig. 6b. As predicted by the numerical simulation, the intensities of the sidebands do change in equal measure with the phase variation. The slight phase shifts between the displayed curves and the mismatch of the magnitude of variations of the three curves were attributed to higher-order dispersion and Raman effects as in the numerical simulations.

5 Second-order modulation instability

The uniform phase dependence of the growth rates of the sidebands changes by seeding with two frequency modes which are not symmetrically spaced around the pump frequency, but which lie on the same side of the pump. Considering a pump peak power of $P_0 = 370$ W, and two seed fields at $\nu_{-1} = -10.5$ THz and $\nu_{-2} = -21.0$ THz, each with an average power of $\bar{P}_{\text{Seed}} = \frac{1}{1000}\bar{P}_0$ (with $\bar{P}_0$ denoting the average pump power of 58 mW), simulations were executed. Note that the second seed frequency is a harmonic of the first ($\nu_{-1} = 2\nu_{-2}$). Figure 7a shows the revealed intensities of the first two sideband pairs as a function of the phase of the pump. To quantify the spectral change due to the second seed pulse, the intensity signals are normalized to the respective intensity signals obtained

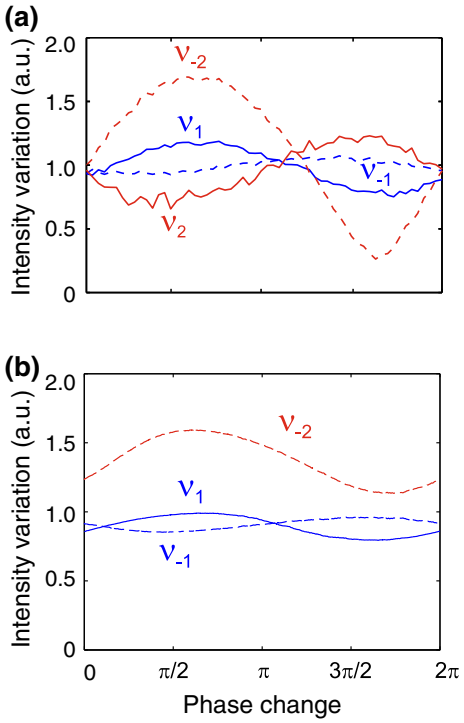

Fig. 7 Simulated (**a**) and measured (**b**) intensity variation of sidebands $\nu_{\pm 1}$, ν_{-2}, seeded with two seed fields at $\nu_{-1} = -10.5$ THz and $\nu_{-2} = -21.0$ THz

for the case of only one seed at ν_{-1} (not shown here, equal to Fig. 6a). In Fig. 7a, revealed by our numerical model, the intensities change with the phase as well, but the intensities evolve contrary, i.e., whereas the intensity of ν_1 increases the intensity of ν_{-1} decreases and vice versa (the same applies for ν_2 and ν_{-2}). Thus, the intensities of the two partners of a sideband pair (e.g. ν_1 and ν_{-1}) vary anti-symmetrically with the phase, resulting in an asymmetric spectral distribution. In the same way, adjacent sidebands (i.e., ν_{-1} and ν_{-2}) also vary anti-symmetrically, which is in total contrast to first-order MI dynamics, in which the sidebands vary symmetrically. Figure 7b shows the same diagram, but deduced from an experiment with the same parameters. As predicted by the simulation, the intensities of the respective sideband pairs do evolve contrarily with the phase variation. The measured intensity of the first two sidebands changed by 20, whereas the intensity of the third sideband changed by 40 compared with the phase-independent signals obtained for the case of only one seed at ν_{-1}. In contrast to the phase dependence of a first-order MI presented in Sect. 3 (Fig. 6), the growth rates of adjacent sidebands are anti-correlated in this case.

A phase-dependent evolution was not observable, when choosing the second seed frequency to $\nu_{-3} = -31.5$ THz, which was located outside of the MI gain curve. In this case, the MI dynamics are solely defined by the first seed frequency mode, showing again no phase dependence. This fact excludes the observed phase-dependent effect from being of interferometric character. Thus, the observed phase-dependent behavior is a clear evidence and a first experimental proof of phase-controlled second-order-like MI dynamics.

It is worth to emphasize again the difference between the phase dependence of a first-order MI and of a second-order MI: as shown in Fig. 6b, a first-order MI, excitable by two seed frequencies (ν_{-1} and ν_1) symmetrically spaced around the pump frequency, exhibits a uniform phase dependence of the sidebands. Consequently, the spectral energy across the sidebands can be increased or decreased, but the spectral distribution cannot be changed with the phase, retaining the symmetry properties of the spectrum. In a second-order MI, as shown in Fig. 7, two sidebands, forming a pair, vary anti-symmetrically with the phase. Thus, the spectral distribution can be changed, leading to an asymmetric spectral distribution.

Besides the spectral placement of the seed pulses, the power of the seed pulses was manifested as another crucial parameter to observe phase-dependent second-order MI dynamics. Therefore, in order to enable the comparison of measured phase-dependent intensity variations for different seed powers, we quantified the anti-symmetric variation of two adjacent sidebands by the correlation coefficient, defined as

$$\mathrm{corr}(I_n, I_m) = \frac{E[(I_n - \mu_n)(I_m - \mu_m)]}{\sigma_n \sigma_m}. \quad (2)$$

Here, E is the expected value operator, μ_j is the mean value and σ_j is the standard deviation of the intensity I_j of the sideband ν_j, with $j = \pm 1, \pm 2, \ldots$. The correlation coefficient can adopt a value in the interval $[-1; 1]$, with a value of 1 denoting perfect correlation and a value of -1 denoting perfect anti-correlation. Figure 8 shows the correlation coefficient $\mathrm{corr}(I_{-1}, I_{-2})$ for the signals of ν_{-1} and ν_{-2} as a function of the seed power and the experimental parameters as above. With a correlation coefficient of -0.9, the investigated phase dependence was most distinct for an average seed power of about 1,000 times smaller than the average pump power. The corresponding measured signals were shown in Fig. 7. Increasing the seed power above 1/1,000 of the pump power degraded the correlation, which can be accounted for by the onset of soliton dynamics interfering with the MI evolution, as a higher seed power reduces the propagation length up to the point, at which the pulse splits into individual soliton-like subpulses. Also, lowering the seed power below 1/1,000 of the pump power led to a reduced correlation due to a lower seed-power-to-noise ratio, which degraded the influence of the seed field. Decreasing the seed-to-pump power ratio below 1/10,000 suppressed the phase dependence of the

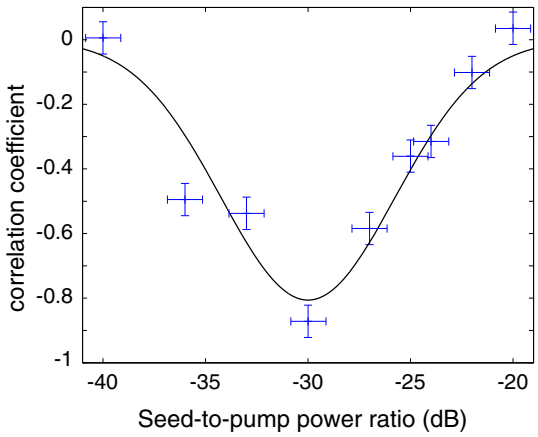

Fig. 8 Correlation coefficient (*blue crosses*) of the measured intensities of the sidebands ν_{-1} and ν_{-2} as a function of the seed power for a MI seeded with two seed fields at $\nu_{-1} = -10.5$ THz and $\nu_{-2} = -21.0$ THz. The *black solid line* is drawn to guide the eye

sidebands. To illustrate the outlined tendency, caused by the competition between seeded MI, noise-driven MI and soliton dynamics, we fitted the solid curve to the data points in Fig. 8.

6 Conclusion

We were able to show experimentally that MI displays a phase-dependent evolution, when stimulating the process with two seed fields, both of which are lying under the gain curve. Specifically, if the second modulation frequency matched a harmonic of the first modulation frequency, i.e., $\nu_{-2} = 2\nu_{-1}$, an asymmetric evolution of the spectrum was observed. Thereby, this seeding concept provides a novel method to control MI-based frequency conversion and thus bears potential for applications, e.g., in optical parametric amplifiers, the initial pump–seed phase difference could be used as a parameter to control the amplification. Or turning it around, a phase-dependent amplification might constitute a measure for phase changes of a weak seed signal. These applications are especially interesting as dichromatically seeded MI has been reported to exhibit low noise figures [14]. Furthermore, as MI dynamics dominate the initial stage of supercontinuum generation (SCG) in the long-pulse regime, the presented findings should contribute to the understanding of SCG and anticipate a new method to influence SCG. Likewise, the presented results might be important for the understanding of other MI-based field evolutions such as the emergence of rogue waves [15].

References

1. V.E. Zakharov, L.A. Ostrovsky, Phys. D Nonlinear Phenom. **238**, 54 (2009)
2. K. Tai, A. Tomita, J.L. Jewell, A. Hasegawa, Appl. Phys. Lett. **49**, 236 (1986)
3. J.M. Dudley, G. Genty, B.J. Eggleton, Opt. Express **16**, 3644 (2008)
4. M. Erkintalo, G. Genty, B. Wetzel, J.M. Dudley, Phys. Lett. A **375**, 2029 (2011)
5. M. Erkintalo, K. Hammani, B. Kibler, C. Finot, N. Akhmediev, J. Dudley, G. Genty, Phys. Rev. Lett. **107**, 253901 (2011)
6. D. Solli, B. Jalali, C. Ropers, Phys. Rev. Lett. **105**, 233902 (2010)
7. J.M. Dudley, S. Coen, Rev. Mod. Phys. **78**, 1135 (2006)
8. K. Blow, D. Wood, IEEE J. Quantum Electron. **25**, 2665 (1989)
9. G.P. Agrawal, *Nonlinear Fiber Optics*. (Academic Press, London, 2007)
10. O. Martinez, IEEE J. Quantum Electron. **23**, 59 (1987)
11. J.M. Dudley, G. Genty, F. Dias, B. Kibler, N. Akhmediev, Opt. Express **17**, 21497 (2009)
12. M. Droques, B. Barviau, A. Kudlinski, M. Taki, A. Boucon, T. Sylvestre, A. Mussot, Opt. Lett. **36**, 1359–61 (2011)
13. M. Erkintalo, Y.Q. Xu, S.G. Murdoch, J.M. Dudley, G. Genty, Phys. Rev. Lett. **109**, 223904 (2012)
14. Z. Tong, C. Lundström, P. Andrekson, Nat. Photonics **5**, 430 (2011)
15. N. Akhmediev, J. Soto-Crespo, A. Ankiewicz, Phys. Rev. A **80**, 043818 (2009)